Macromolecules

pubs.acs.org/Macromolecules Article

Key Insights into the Differences between Bimodal Crystallization Kinetics of Polyamide 66 and Polyamide 6

Xiaoshi Zhang, John Buzinkai, Evan Quinn, and Alicyn Rhoades*

Cite This: *Macromolecules* 2022, 55, 9220−9231 Read Online

ACCESS | Metrics & More | Article Recommendations | Supporting Information

ABSTRACT: Polyamide 66 (PA66) and polyamide 6 (PA6) share many comparable properties due to their similar chemical structures. However, their crystallization kinetics and morphological differences are not as well understood as other properties. This work establishes the crystallization kinetics and morphology of additive-free PA66 and PA6 at high undercooling conditions using a modified fast scanning calorimetry technique. Two polyamides show similar kinetics profile and morphology, but the transitions associated with polymorphs occur at different temperatures. Regarding kinetics, PA66 always crystallizes faster than PA6 regardless of the polymorphs formed, supported by the temperature-dependent Avrami kinetics coefficients k. Both PA66 and PA6 show a bimodal kinetics profile with a local crystallization rate minimum at 135 and 110 °C, respectively. Apart from the crystallization rate, a sudden broadening of the exothermic crystallization peak is found near the rate minimum. The broadening is described by a drastic change of the Avrami index n from 3 to 2. The morphology at the micro- and nanoscales of polyamides was followed by a polarized optical microscope (POM) and atomic force microscopy (AFM). The POM reveals that both polyamides turn translucent from transparent near the rate minimum. The temperature-dependent AFM micrographs show multistep transitions from amorphous-like morphology, cauliflower-like crystal, crystal aggregates, and lamellar structure after T_c changes from near T_g to above the kinetics break temperature. Although two polyamides have similar molecular weight and the same content of amide groups, the morphological transition in PA66 is found to always be 20 °C higher than in PA6, suggesting a difference in their thermodynamic drive to nucleate. The conclusions drawn from the Avrami analysis in the final part of this study provide a universal explanation of the drastic peak broadening observed in many previously studied thermoplastics.

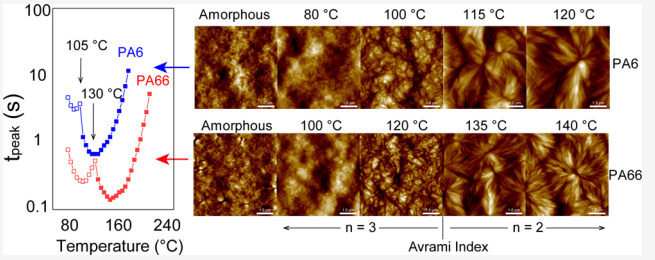

INTRODUCTION

Polyamides were the first semicrystalline synthetic engineering plastics and remain one of the most important thermoplastic materials. Compared to commodity aliphatic plastics, such as polyethylene, the amide groups in polyamides provide hydrogen bonding to bind adjacent chains, yielding a unique combination of high stiffness, good chemical resistance, and high abrasion resistance.

Aliphatic polyamides consisting of methylene sequences (−CH_2−) and amide groups (−NH−CO−) are designated into polyamide-m and polyamide-m,n. The largest volume polyamides for each category discussed above are polyamide 6 (PA6) and polyamide 66 (PA66).[1] Many properties in polyamides are governed by the amide group content. Because both polyamides have two amide groups per 12 backbone carbons, there are small differences between PA66 and PA6 in many properties, including density, glass-transition temperature, tensile properties, and impact strength.[1−3] Furthermore, their blends are miscible due to very similar chemical structures.[4] On the other hand, amide groups in PA66 are alternately reversed along the chain, while in PA6, the amide groups are on the same side of the chain, giving directionality to the chain. This minor difference in the repeating units leads to the major difference between the two polyamides. The lack of directionality affects the entropy change upon melting and is believed to cause PA66 to melt about 40 °C higher than PA6.[1] A direct consequence of high melting temperature is the higher melt-processing temperature required for PA66. Many review articles have often suggested at least a 40 °C increase of the minimal melt temperature to mold PA66 compared to PA6.[3,5] Unlike the well-known large difference in their melting temperatures, the crystallization kinetics differences of PA66 and PA6 have not received similar attention; for example, the International Organization for Standardization (ISO) still recommends employing a similar mold temperature for both polymers during the preparation of test specimens.[5] However, controlling crystallization, a major step of solidification during melt processing, strongly relies on the knowledge of kinetics at

Received: May 20, 2022
Revised: August 20, 2022
Published: October 10, 2022

https://doi.org/10.1021/acs.macromol.2c01059
Macromolecules 2022, 55, 9220−9231

high undercooling and rapid cooling conditions and can help to design an efficient pathway to make products with desired properties. As previously reported, PA66 and PA6 can develop more than one type of crystal depending on the crystallization conditions.[6−8] Amorphous phase due to incomplete crystallization and mesophase formed at low crystallization temperatures undergo an irreversible reorganization to a more stable phase after annealing,[9,10] which is believed to be one of the reasons for part deformation in some high-temperature or high-frequency loading applications.

One of the major challenges of studying polyamide crystallization under processing-relevant conditions is the historical limitations of thermal instrumentation to follow the ultrafast crystallization process, which usually completes within 10 s. This problem can now be solved by the fast scanning calorimetry (FSC) technique. The crystallization kinetics fingerprints of many common thermoplastics have been revealed for the first time.[8,11−15] For example, it was found that the solidification of PA66 and PA6 is extremely fast but behaves differently in their isothermal crystallization and nonisothermal crystallization kinetics.[6−9,16−18]

Many common thermoplastics exhibit a universal bimodal shape of crystallization kinetics when plotted as crystallization time against isothermal crystallization temperature, including PA66 and PA6.[6−8,12,14,19] Crystallization kinetics exhibit two local crystallization time minima between the glass-transition and melting temperatures in the bimodal shape kinetics. The crystallization peak time between the minima shows a break in kinetics at a temperature, named the crystallization kinetics break temperature, as will be shown later in Figure 2. A common interpretation for this phenomenon is that the polymer undergoes a drastic change in nucleation mechanism from homogeneous nucleation at low crystallization temperatures to heterogeneous nucleation at high crystallization temperatures.[20] This mechanism was initially developed to explain that crystallization within submicron droplets occurs at much larger supercooling than in the bulk sample. Switching the nucleation mechanisms explains the case of iPP by De Santis et al. very well.[12] The Avrami index changes from 4 to 3 near the crystallization kinetics break temperature, suggesting spherulitic (3D) growth of iPP changes from spontaneous to instantaneous nucleation with increasing crystallization temperature. This mechanism is also discussed in the former study of PA66 and PA6,[6−8] explaining the crystallization kinetics break. However, this previous work relies on observations of confined polymer droplets, and it should be noted that the crystallization kinetics of droplets strongly depend on other factors, including spatial confinement effect (volume),[21,22] the roughness of the substrate,[23] the ratio between numbers of droplets and active heterogeneity,[22] etc. The validation of this mechanism in bulk polymer matrices still requires more evidence. For example, one can study the crystallization kinetics of additive-free polymer in a bulk whose basis of having heterogeneous nucleation does not exist. In some works, an alternative explanation of "polymorphism transition" is used to explain the break in crystallization kinetics.[6,8,13,19,24,25] Unlike switching nucleation mechanisms, pure polymer without nucleants can have bimodal kinetics in this theory, as long as the temperature coefficient of crystal growth differs significantly in different crystalline forms. Under this explanation, one should expect that the polymer will have different unit cell packings and morphologies on the two sides of the kinetics break. Former studies of FSC-prepared PA66 and PA6 samples have confirmed that the polymorphism transition occurs near the kinetics break.[7,8] On the other hand, the AFM morphology on FSC-prepared samples has been difficult and expensive to obtain because the FSC sensor needs to be fractured.[7,9,17,26] Recently, a method has been developed to scan FSC-prepared samples in AFM without damaging the sensor.[8] The use of this new method enables the authors to examine the possible morphological change induced by crystallization temperature near the kinetics break on the same area of the sample.

Another feature observed by FSC in the isothermal crystallization kinetics of thermoplastics is the sudden broadening of the exothermic isothermal crystallization peak near the kinetics break. It is noted that this sudden broadening has been found in both PA66 and PA6 in the former works.[6,8] Unlike the temperature-dependent t_{peak} or $t_{0.5}$, less effort has been made to explain this phenomenon, not to mention a proper explanation. This is probably due to only a few works reporting the 3D waterfall plot or plot series of heat flow against temperature and time.[6,8,12,14] A universal explanation for such behavior is highly desired.

In this work, the overall crystallization kinetics of PA66 and PA6 at high undercooling conditions are studied and compared. Both polyamide samples are additive-free resins from commercial production processes and are believed to contain extremely low or no nucleant species. The two polyamides have the same molecular weight and solution viscosity to minimize the potential difference in chain mobility. The selection of commercially produced polyamides can help the authors to validate the nucleation change mechanism by eliminating the influence of heterogeneous nucleants in the system. Additionally, both polyamides' temperature-dependent Avrami kinetics coefficient k and Avrami index n are analyzed. The morphology using POM and AFM in a wide temperature range is first thoroughly investigated. Lastly, the Avrami equation discussions provide a universal explanation of the rapid peak shape change observed in many thermoplastics.

EXPERIMENTAL SECTION

Materials and Preparation. Materials used for this study are commercial prime resin grade U4803 from INVISTA and commercial prime resin grade Ultramid B27E from BASF. INVISTA U4803 is an additive-free PA66, and Ultramid B27E is an additive-free PA6. The moisture level of both grades was 0.07% prior to experiments. The measured solution viscosity for U4803 and B27E is about 2.7 RV for 1.0 w/v % solution in 96% sulfuric acid or VN of about 150 mL/g, as determined by ISO 307 with 0.5 w/v % solution in 96% sulfuric acid. Both polyamides have a viscosity-determined number-average molecular weight of about 16 kg/mol. A PDI value of 2 is expected for both grades, as previously established by Oshinski et al.[27] Pellets of PA66 and PA6 were microtomed to obtain thin sections with a thickness of 12 μm for FSC experiments. Thin sections were then further cut to obtain a lateral dimension of around 50 μm using a scalpel under a Leica stereomicroscope.

Measurements. *Fast Scanning Calorimetry.* Modified UFS1-type chips were used for calorimetry and subsequent morphological analyses. More details of the modified chip can be found in the previous paper.[8]

Sample preparation and calorimetric analyses were performed using a Mettler Toledo Flash DSC1 with a Huber TC100 two-step cooling intracooler. The FSC sensors were conditioned and temperature-corrected before loading the specimen. In all instances, the calorimeter was purged with dry N_2 gas. Thin specimens were loaded on the center of the chip and then prepared in their molten state inside the FSC. The thickness of the sample is further reduced using a

https://doi.org/10.1021/acs.macromol.2c01059
Macromolecules 2022, 55, 9220−9231

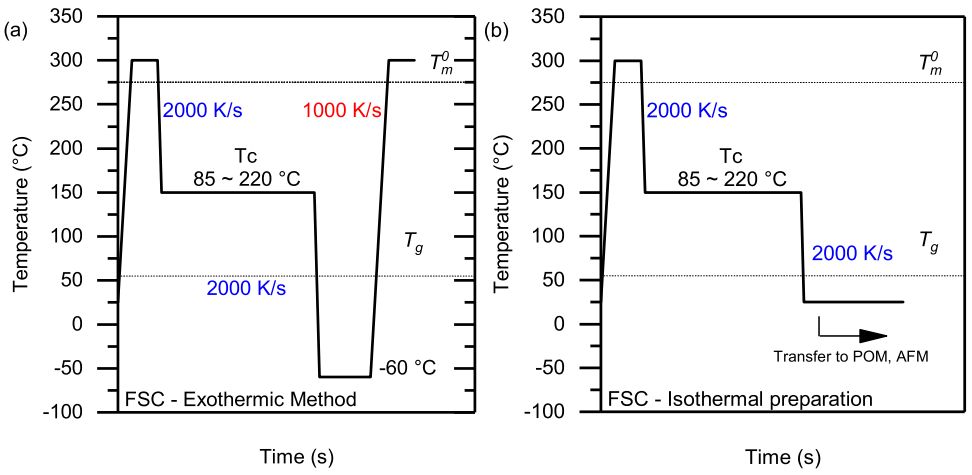

Figure 1. Temperature−time protocols used in FSC for (a) isothermal crystallization for exotherm analysis and (b) isothermal sample preparation.

wire to spread the molten specimen over the heating zone. Nitrogen flow was used to mitigate potential degradation or oxidation. Crystallization kinetics information was extracted directly from the exothermic heat flow, as illustrated in Figure 1a. To obtain exothermic heat flow, the sample was initially heated to 300 °C for 0.5 s to erase thermal history. The temperature for melting is higher than the reported values of equilibrium melting temperature of PA6 260 °C[28] and PA66 275 °C.[29] Then, the melt was cooled to the crystallization temperature (T_c) at a rate of 2000 K/s. The sample was kept at the selected isothermal crystallization temperature for 30 s to allow complete crystallization.

The FSC chip was also used as a micro hot stage for subsequent polarized optical microscope (POM) and atomic force microscopy (AFM) experiments, as illustrated in Figure 1b. The samples were melted at 300 °C for 0.5 s to eliminate thermal history, cooled to the isothermal crystallization temperature at 2000 K/s, and maintained for 2 min to allow complete transformation. Then, samples were then quenched to 25 °C at a cooling rate of 2000 K/s. The rapid cooling process can freeze the material structure because 25 °C is below the T_g of both samples studied (52 °C for PA6 and 53 °C for PA66).[30] The sample on the sensor was then transferred into a different instrument for measurements. After measurements, the sensor and sample were reinserted into the FSC for subsequent thermal treatment. It is important in this study that the same specimen is tested repeatedly at different temperatures for subsequent imaging, as there are no questions due to (1) differences in thermal lag due to changes in sample geometries or (2) differences regarding nucleation potential from sample location/selection.

Polarized Optical Microscopy. The polarized micrographs of PA66 and PA6 after preparation using FSC were collected directly on the chip using a Leica DM2700P microscope and a Leica DFC7000T camera using transmission mode. To enhance the contrast in weakly birefringent spherulites, a retardation plate was used. POM micrographs were processed and analyzed using ImageJ from the National Institutes of Health (NIH).

Atomic Force Microscopy. AFM micrographs were collected using a Bruker Dimension ICON atomic force microscope with a NanoScope V controller. Samples were scanned directly on the chip using a ScanAsyst-Air probe with a tip radius of 2 nm, a nominal resonant frequency of 70 kHz, and a nominal spring constant of 0.4 N/m under PeakForce QNM mode at an ambient temperature. Height, height error, and peak force error channels were collected. NanoScope Analysis Software provided by Bruker and ImageJ from NIH were used for AFM image processing and analysis.

RESULTS AND DISCUSSION

Overall Isothermal Crystallization Kinetics. Plots of heat flow against crystallization times at different crystallization temperatures for PA66 and PA6 are displayed in Figure 2. A common feature among both polyamides is their bimodal temperature-dependent kinetics, as previously reported in different grades of PA66[6,7] and PA6.[8,31] The crystallization peak times of PA66 and PA6 extracted from waterfall plots are compared in the same figure. For PA66, two crystallization time minima are found at 110 and 155 °C, with a local peak time maximum (local rate minimum) observed at 130 °C. The slowdown of crystallization kinetics below 110 °C and above 155 °C can be explained by the reduced mobility and reduced thermodynamic drive when the temperature is close to T_g and T_m^0, respectively.[32] For PA6, a similar slowdown of crystallization takes place between 95 and 110 °C. Unlike PA66, the local crystallization rate minimum appears at a much lower temperature of 105 °C. The kinetics observed in additive-free polyamides indicate that the nucleant is not likely to be the major reason causing bimodal kinetics. Another feature extracted from both heat flow and temperature waterfall plots is the drastic change of the curve shape: all peaks below the local rate minimum are sharper than those above. This feature is evident in both polyamides but was barely mentioned in the past.

The Avrami equation is often used to extract the Avrami index, n, to quantitatively describe growth dimension change or nucleation mechanism change using DSC data.[33,34] Compared to DSC exothermic heat flow, FSC exothermic heat flow has a much shorter induction time and uneven baseline, requiring more careful data processing. All of the isothermal crystallization exotherms with baselines for PA66 and PA6 are displayed in Figures SI 1 and 2. A nonlinear baseline was used to accommodate the variation of heat flow associated with sensor thermal lag and material heat capacity change during crystallization. From the exothermic heat flow and baseline, the integrated heat of fusion ΔH and final heat of fusion from primary crystallization ΔH_{final} were measured. The weight fraction, W_c, was then calculated using the formula, $W_c = \frac{\Delta H}{\Delta H_{final}}$. Since the Avrami equation describes the volumetric fraction change against crystallization time, the volumetric fraction, V_c, follows

$$V_c = \frac{W_c}{W_c + (\rho_c/\rho_a)(1 - W_c)} \quad (1)$$

ρ_a and ρ_c denote the fully crystalline and mobile amorphous densities, respectively. The ρ_c and ρ_a of PA66 are 1.24 and 1.09

https://doi.org/10.1021/acs.macromol.2c01059
Macromolecules 2022, 55, 9220−9231

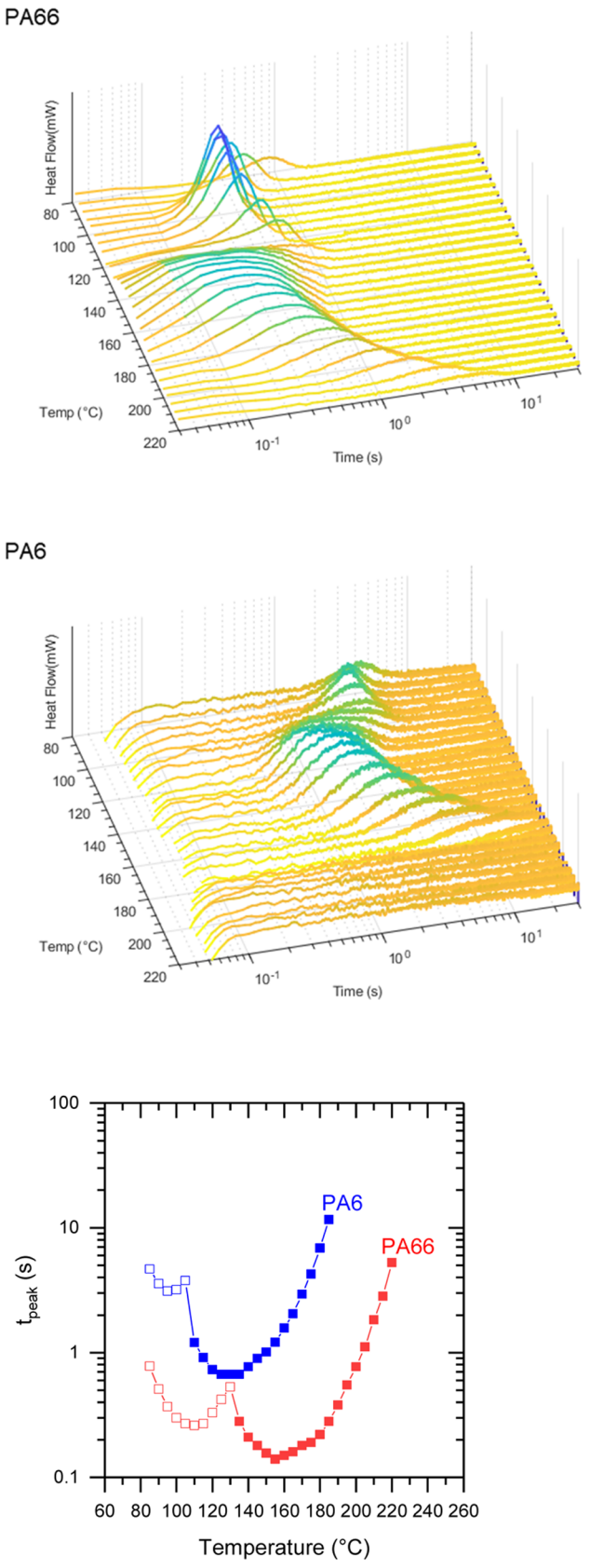

Figure 2. Waterfall plot of the heat flow rate as a function of time, obtained during isothermal crystallization of (top) PA66 and (middle) PA6 at temperatures between 80 and 220 °C. (Bottom) Overall crystallization kinetics of PA66 and PA6. The exothermic heat flow is positive (directed upward).

g/cm^3, respectively.[35] The crystalline and amorphous phases of PA6 have densities of 1.23 and 1.10 g/cm^3, respectively.[36]

Then, V_c can be expressed by the Avrami equation with the Avrami index n and Avrami kinetic coefficient k

$$1 - V_c(\tau) = \exp(-k\tau^n) \tag{2}$$

Importantly, the crystallization time used in the Avrami equation, τ, is not the same time recorded by the instrument, t. The induction time until the onset of crystallization, t_0, should always be subtracted since the Avrami equation only describes the phase transition after crystallization initiates.[33,34,37] Improper use of time in the Avrami equation may lead to an unrealistic Avrami index value higher than 5.[38] Accurate t_0 values are measurable for both polyamides except for the temperature region between 140 and 190 °C for PA66, as illustrated in Figure SI 1. Although many attempts were made to give proper baselines to predict t_0, Lorenzo et al. suggest that improper baselines could lead to significant relative errors of the Avrami index after carefully examining many incomplete runs.[37] In this case, the authors assume that the PA66 induction time in T_c between 140 and 190 °C is 0. From now on, the analyses based on the data collected in this temperature region are marked differently. After introducing t_0, eq (2) then should be written as

$$1 - V_c(t - t_0) = \exp[-k(t - t_0)^n] \tag{3}$$

Applying a double natural logarithm operation on both sides, eq (3) becomes

$$\ln[-\ln[1 - V_c(t - t_0)]] = \ln(k) + n\ln(t - t_0) \tag{4}$$

Avrami plots for PA66 and PA6 crystallized in two different temperature regions are displayed in Figure 3. Panels (a) and (b) are for the data of PA66, and panels (c) and (d) are for the data of PA6. In panels (a) and (c) of Figure 3, representing the low T_c kinetics, the fitted data follow a slope of 3, while in panels (b) and (d), the slope is near 2. The change of slope occurs within a temperature range of less than 10 °C. The Avrami plots for PA66 crystallized between 140 and 180 °C are displayed in Figure SI 3. The slopes in T_c between 140 and 180 °C are slightly below 2; these values are expected to be near 2 if accurate induction times could be captured.

The n and k across the entire crystallization temperature region for both polyamides are compared and summarized in Figure 4. The k, n values and the induction time t_0 for both polyamides are summarized in Tables SI 1 and 2. Avrami index n values near 3 are obtained in the temperature region below 130 °C for PA66 and 105 °C for PA6. These low-temperature regions were inaccessible by DSC in the past and are first studied by FSC in this work. One would expect all mesophases to have a universal value for the Avrami index n since mesophases from different thermoplastics have shown similar diffractograms and morphology.[7,8,13,19,39] Surprisingly, two polyamides have an n value of 3, while iPP has a value of 4, as previously reported by De Santis and Schick et al.[12] In both studies, the induction time was properly subtracted. The difference must then be caused by inherent differences in behavior of the polymers rather than the data analysis. Above the low-temperature regions, a step drop of n from 3 to 2 occurs in both polyamides. As expected, the step change temperatures are also close to the observed local crystallization rate minimum in Figure 2. A reduction of 1 in the n value agrees with the previous work on iPP at the transition temperature.[12] An n value of 2 in polyamides is further

https://doi.org/10.1021/acs.macromol.2c01059
Macromolecules 2022, 55, 9220−9231

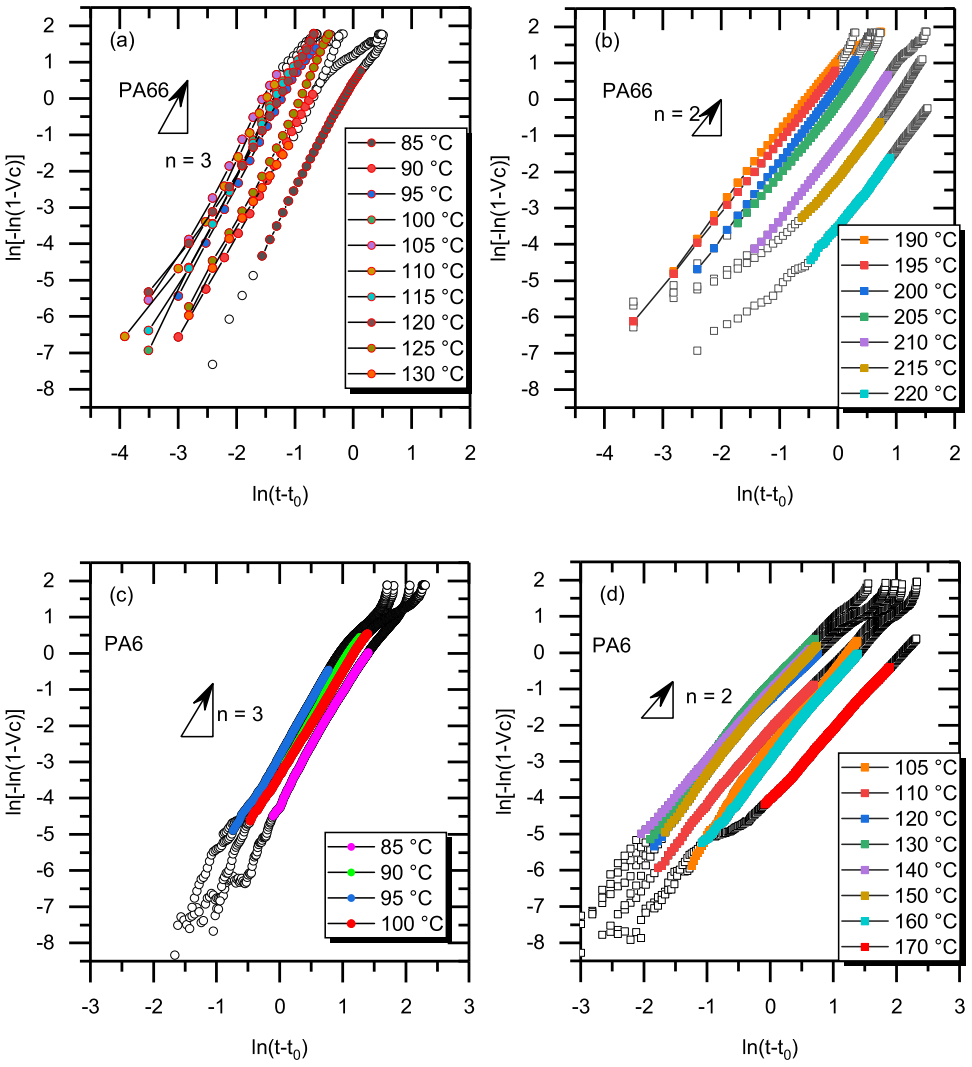

Figure 3. Avrami plot of PA66 experimental data (open symbols) obtained from (a) isothermal crystallization at and below 130 °C and (b) isothermal crystallization at and above 190 °C. Avrami plot of PA6 experimental data (open symbols) obtained from (c) isothermal crystallization at and below 100 °C and (d) isothermal crystallization above 100 °C. The filled symbols represent the data used for the Avrami fit.

supported by previous Avrami analyses[40−42] since high-temperature kinetics data were accessible by DSC. An n value of 3 at lower temperatures suggests that the polymer is either crystallizing under spontaneous nucleation with growth in 2D (disk shape) or under instantaneous nucleation under 3D geometry, while an n value of 2 suggests that both polyamides grow under instantaneous nucleation with a growth dimensionality of 2.[43] The physical meaning of n is still under debate. In the review by Piorkowska et al., they suggest that the n value is just the best adjustable parameter for fitting,[44] with no direct correlation to physical microstructures.

Temperature-dependent k values for both polymers, as displayed in Figure 4, also show a clear break near the n step change temperature. A break in k suggests different temperature coefficients of crystal growth. This agrees with the explanation of polymorphism transition concluded from WAXS and FTIR.[7,8] The k value of PA66 is always at least 1 order of magnitude larger than PA6 and 2−3 orders over most of the temperature range for crystal formation, indicating far-faster crystallization.

Morphological Changes. Polarized optical micromorphology of PA66 after isothermal crystallization between 70 and 200 °C was previously studied by Gohn et al.[7] The optical micrographs obtained using reflected polarized light mode show a change of opaqueness when the crystallization temperature crosses the region between 110 and 120 °C. The transition temperature is below the observed rate minimum of 135 °C.[7] In this study, polarized optical micrographs were collected using transmission mode, as displayed in Figure 5. Compared to reflection mode, the use of transmission mode can further enhance the contrast to differentiate small structures from the dark background. Amorphous polyamide samples prepared by ultrafast cooling (2000 K/s) are found to be transparent. This observation is similar to other transparent amorphous samples, such as PC, PMMA, and PS, since the amorphous polymer matrix is isotropic. Interestingly, polyamides formed at low T_cs are also transparent under polarized light, which is quite different from the expected translucent or opaque appearance since visible light is scattered at the boundaries between amorphous and crystalline regions. The subsequent melting curves have confirmed the formation of crystals, as displayed in Figure SI 4. Transparent morphology is only possible if the crystal sizes are below the wavelength of visible light or the refractive

https://doi.org/10.1021/acs.macromol.2c01059
Macromolecules 2022, 55, 9220−9231

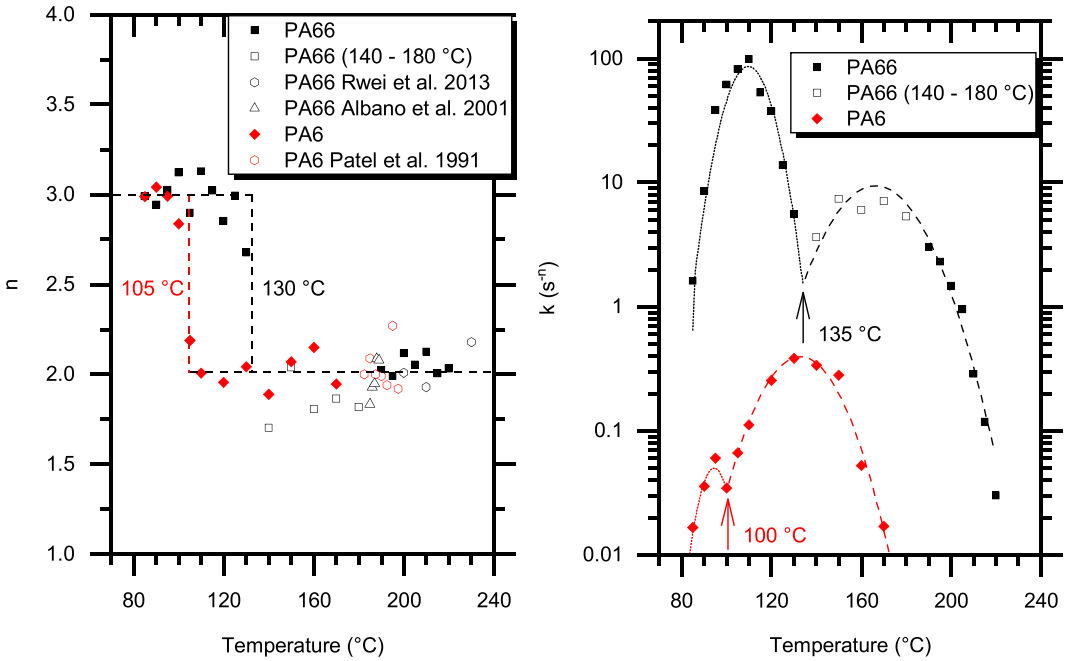

Figure 4. (Left) Avrami index *n* and (right) Avrami kinetic coefficient *k* of PA66 and PA6 in a wide crystallization temperature range. Data of PA66 analyzed using incomplete exothermic heat flow; literature values for n are also added. Dash lines added in the Avrami kinetic coefficient plot are calculated by the second-order polynomial fitting.

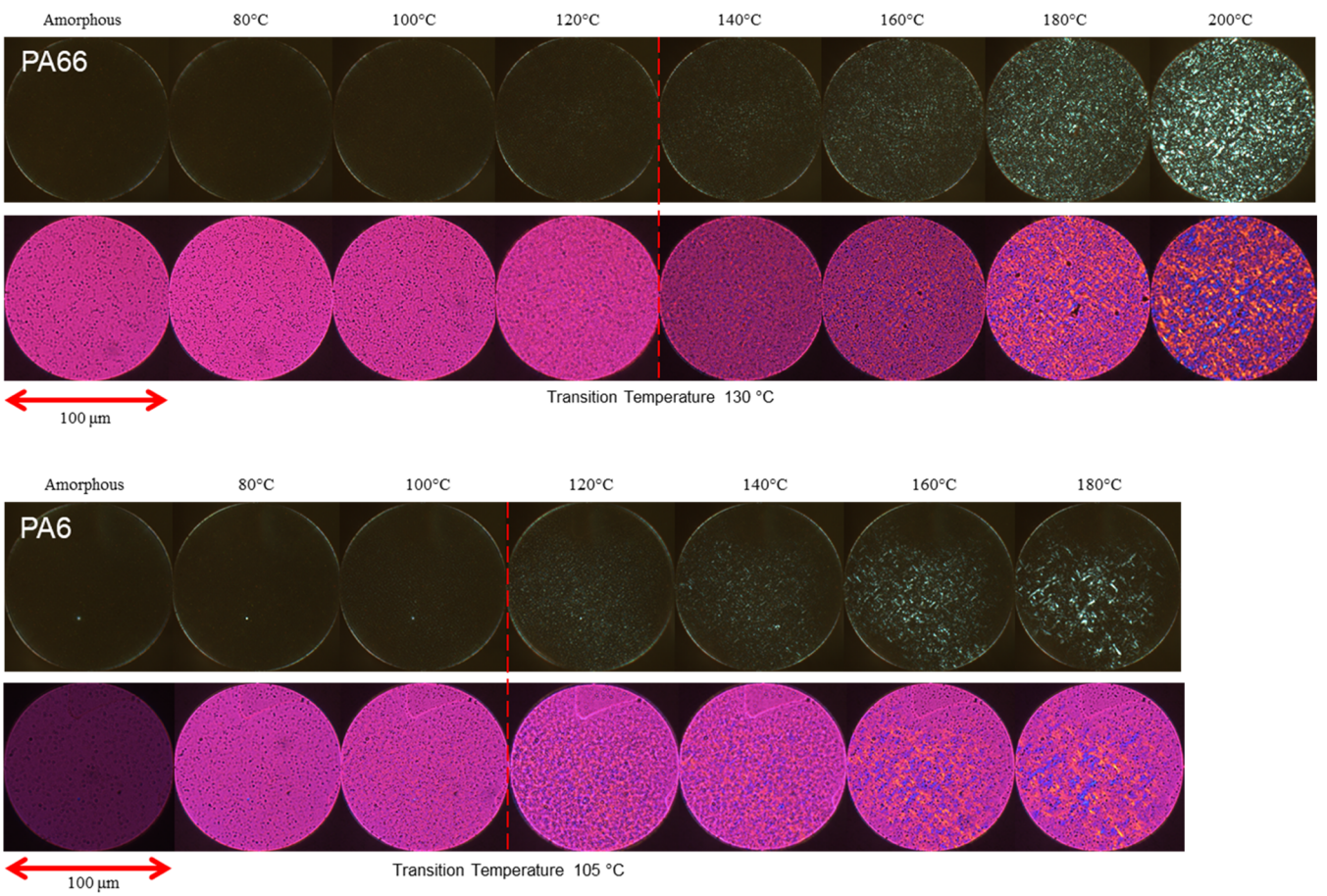

Figure 5. Representative polarized optical micrographs of (top) PA66 and (bottom) PA6 isothermally crystallized at indicated temperatures. The opening on the modified chip for imaging is 100 μm. The black specks in the color-enhanced micrographs are from the amorphous SiN_x membrane and are mostly filtered by polarized light.

https://doi.org/10.1021/acs.macromol.2c01059
Macromolecules 2022, 55, 9220−9231

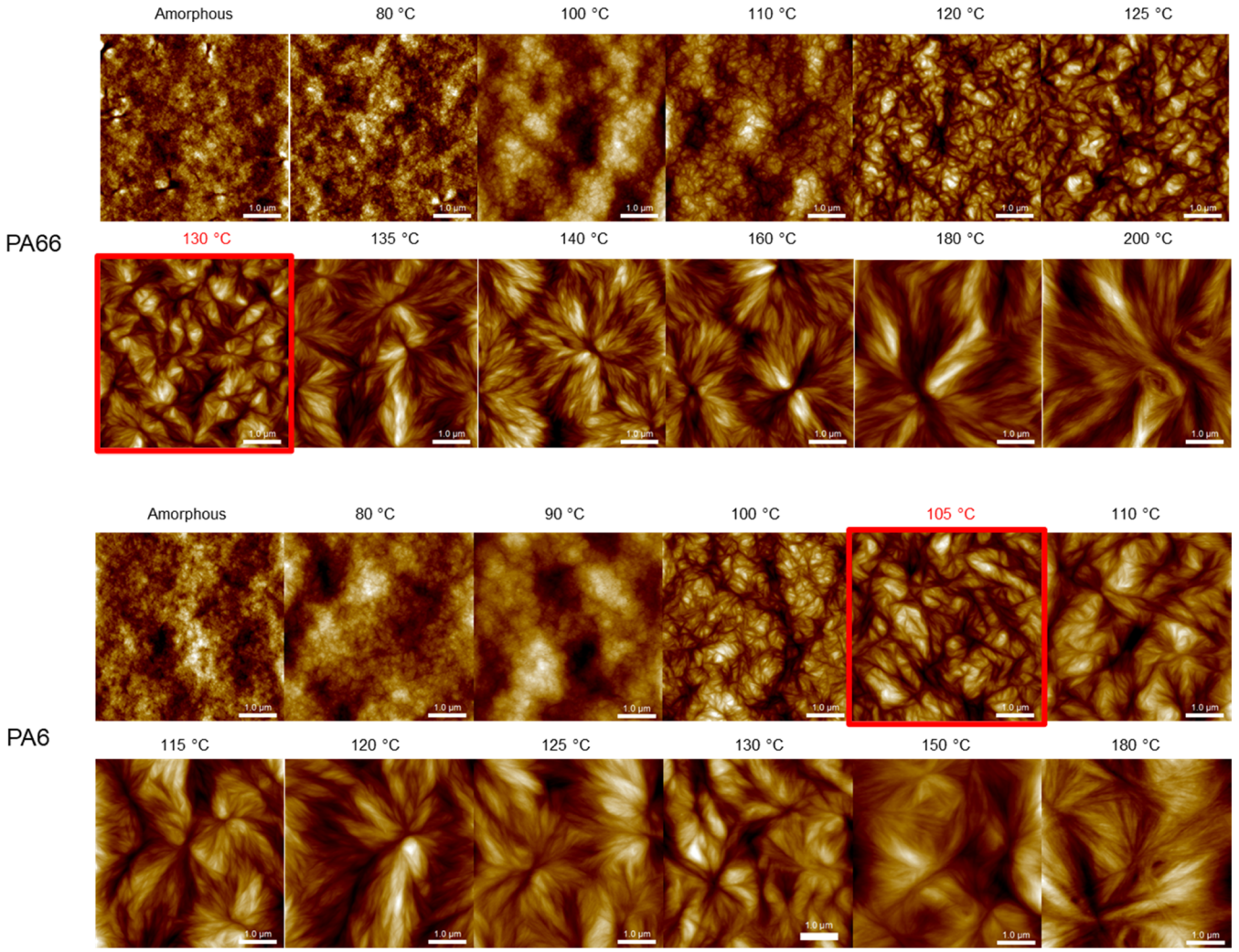

Figure 6. AFM micrographs of (top) PA66 and (bottom) PA6 crystallized at indicated crystallization temperatures. Micrographs at a kinetics transition temperature of 130 °C for PA66 and 105 °C for PA6 are highlighted.

indices (RIs) of amorphous and crystal domains are close.[45] As T_c increases, the polarized micrographs of both polyamides show a transition from totally dark to having some visible crystals. The transition takes place near the local rate minimum from kinetics.

Possible reasons for having visible crystals crystallized at high T_cs could be either increasing crystal size or a larger refractive index difference between the amorphous and crystalline domains. Typically, researchers attribute this to nucleation density, but this might be too simplistic. The observations in this study support both explanations. At the same temperature where crystals become visible, color-enhanced micrographs collected using a retardation plate show blue and yellow interference colors. Not only the contrast and brightness, but the domain size also increases at higher T_cs. As will be discussed for AFM micrographs, the crystal size increases significantly at higher T_cs. An increased refractive index difference is also expected. In a series of works by Fouda et al., refractive indices of PA66 and PA6 were measured after annealing.[46,47] Both polyamides have higher RI after annealing at elevated temperatures. The onset of the upturn temperature is near 120 and 110 °C for PA66 and PA6, respectively. In this study, the temperature where crystals become visible is near the polymorphism transition and Avrami index change temperature. Higher density causes a higher refractive index in a polymer.[48] Polymorphism transition from mesophase to the thermodynamic stable phase results in a more densely packed crystal phase with higher mass density,[35,36] consequently leading to higher contrast.

The maximum resolution of POM is limited to ~370 nm, as calculated according to the Rayleigh criterion using a numerical aperture of 40× objective (0.75) and a light wavelength (λ = 550 nm) with a plan fluorite objective. A different instrument is required to explore morphology at a smaller scale. Gohn et al. used AFM to study the PA66 morphology after FSC preparation.[7] The method used requires detachment of the SiN_x membrane from the silicon frame and the ceramic housing. Morphology was only studied at two temperature extremes far from the local crystallization rate minimum. It was hypothesized that a drastic morphology transition from homogeneous nucleation to heterogeneous nucleation occurs at the local rate minimum. In our previous work on PA6, a new way of AFM experiments was developed to scan FSC-prepared samples directly on the chip without detaching the membrane.[8] An interesting continuous nanoscale morphological change with temperature was obtained. The same method is utilized to fully map the morphological evolution of PA66. Additionally, more AFM images of PA6

https://doi.org/10.1021/acs.macromol.2c01059
Macromolecules 2022, 55, 9220−9231

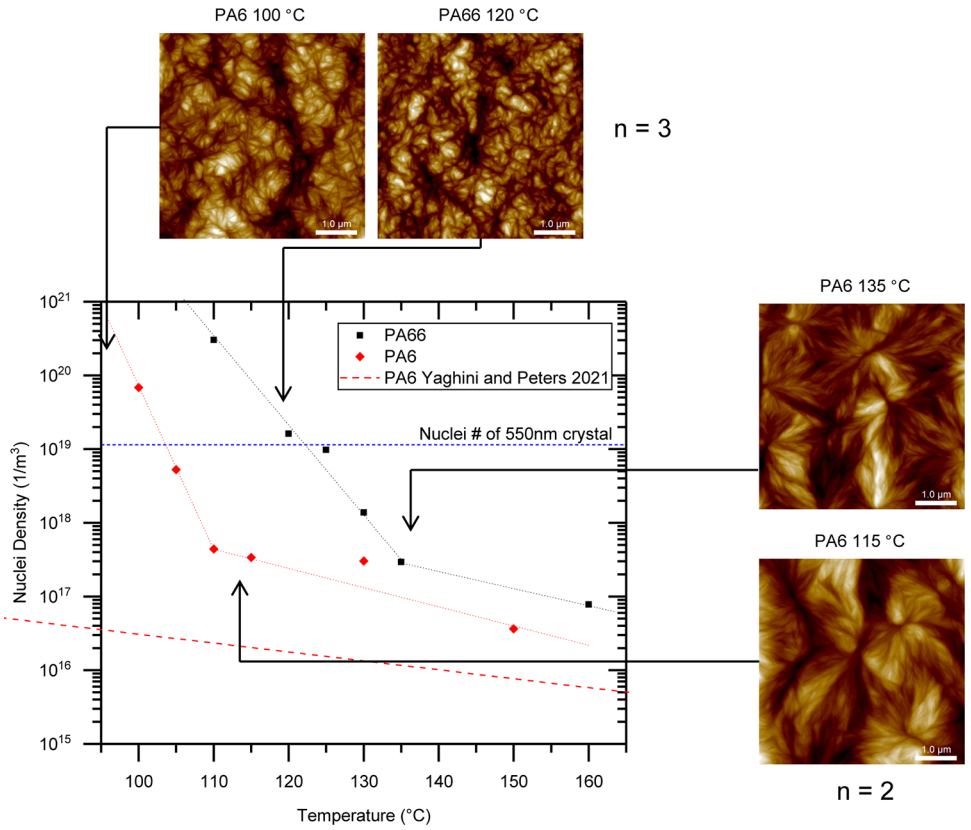

Figure 7. Estimated nucleation density of PA66 and PA6. Dotted lines are added to emphasize the abrupt changes and are not from data fitting. PA6 heterogeneous nucleation density data from Yaghini and Peters[50] is added for comparison. Nuclei density of crystal with a size of 550 nm is added. Data above the blue dotted line has a crystal size smaller than the light wavelength.

crystallized near the polymorphism transition region between 100 and 125 °C were collected, as shown in Figure 6.

The morphological evolution of PA66 crystals displayed in Figure 6 is similar to that previously found in PA6.[8] Both polyamides go through multistage morphological changes from amorphous-like morphology, cauliflower-like crystals, crystal aggregates, and lamellar structure after T_c changes from near T_g to above the kinetics break temperature. The only difference between the two polymers is the temperature where the morphological transition occurs. At a crystallization temperature of 80 °C, only 25 °C above the T_g for both polyamides, PA66 mesophase has an amorphous-like morphology, whereas PA6 mesophase starts to develop a cauliflower-like morphology that is not seen in PA66 until a higher T_c of 100 °C. According to the Turnbull−Fisher equation, such low crystallization temperatures are traditionally regarded as the chain mobility-controlled region.[32] From an experimental setup point of view, these materials were carefully prepared and selected such that the two polyamides are expected to have similar chain mobility since they have the same molecular weight, amide group content, and glass-transition temperature. Hence, the difference in morphology is most probably caused by different driving forces of nucleation even at such low temperatures. One possible difference in their nucleation driving forces is the thermodynamic property of the mesophase or, more specifically, the equilibrium melting temperature of the mesophase. As previously mentioned, one of the major differences between isomers of PA6 and PA66 is the directionality, giving a 40 °C higher melting temperature of PA66.[1] The lack of directionality in PA66 experiences lower entropy change upon melting. For mesophase, PA66 and PA6 have a similar pseudo-hexagonal packing with no long-range order.[7,8] At the same time, the difference in the directionality still exists due to their intrinsic repeating unit structure difference, giving a lower melting temperature of PA6 mesophase. The AFM morphology suggests a 20 °C difference between their undercooling values ($\Delta T = T_m^0 - T_c$). Apart from 20 °C, the T_c difference in obtaining cauliflower-like crystals in PA66 and PA6, crystal aggregates, and lamellar morphology are obtained at 120 and 135 °C for PA66, while at 100 and 115 °C for PA6; 135 and 115 °C are also near the kinetics break temperatures in PA66 and PA6.

Although the morphology of both polyamides crystallized at T_c extremes of 70 and 200 °C agrees with previous AFM observations that were used to support the nucleation switching mechanism,[7,19] the crystal aggregate morphology obtained just below the kinetics break temperature is hard to categorize into either the homogeneous nucleation or heterogeneous nucleation mechanism. Our previous discussion of the PA6 morphology transition at low temperatures proposed that crystal growth transitions through multiple stages from the mesomorphic layer formation to the granular crystal layer and to lamellar, as described by Strobl's multistage growth model.[8,49] The mesophase is quickly replaced by a more stable polymorph when the molecular chains finally form lamellae. It was believed that the thickening process requires a continuous rearrangement of the chain sequence at the cost of mobility. The PA66 multistage morphology can also be interpreted using the same explanation. However, one should notice that the transition to different morphology stages occurs

https://doi.org/10.1021/acs.macromol.2c01059
Macromolecules 2022, 55, 9220−9231

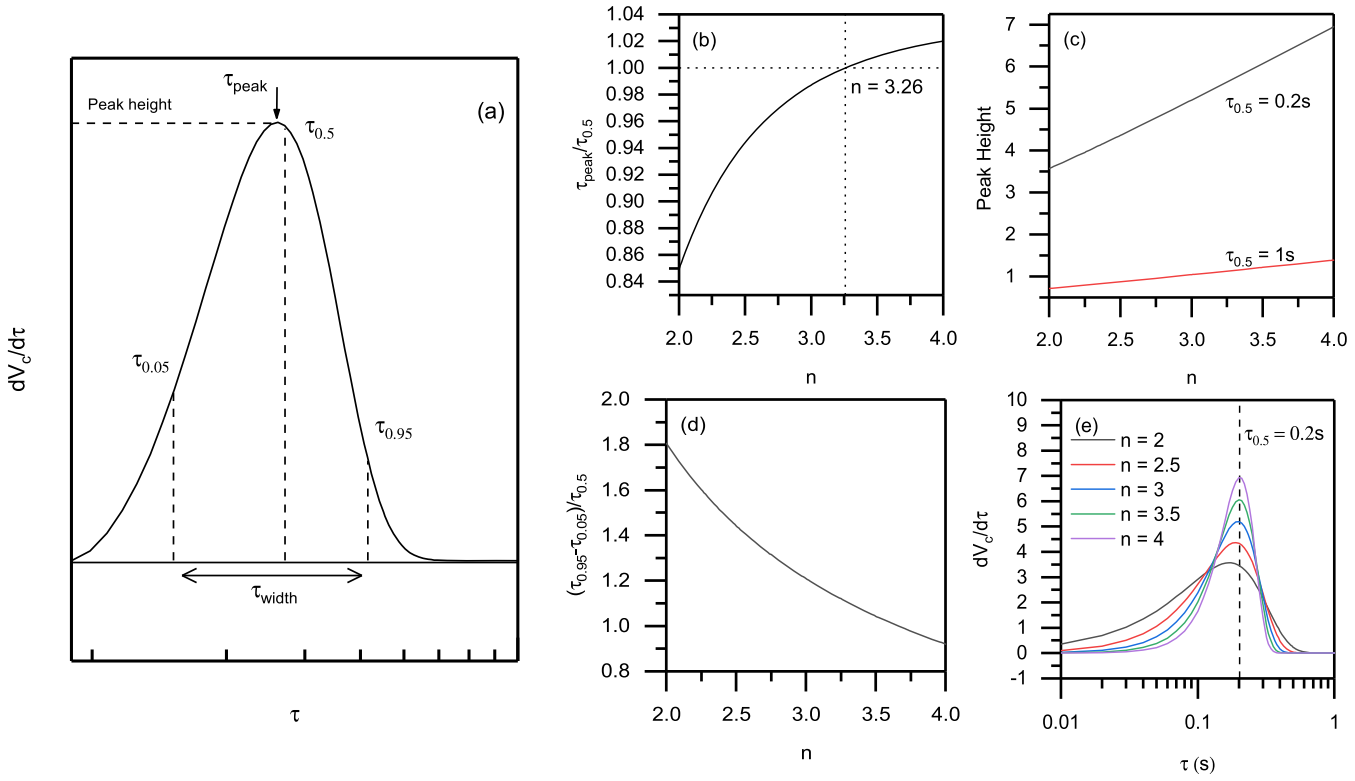

Figure 8. (a) Parameters discussed in the Avrami analysis. *n*-Dependent value of (b) the ratio of τ_{peak} and $\tau_{0.5}$, (c) peak height $\left(\frac{dV_c\ (\tau = \tau_{peak})}{d\tau}\right)$ with $\tau_{0.5}$ of 1s and 0.2s, (d) the ratio of peak width τ_{width} $(\tau_{0.95} - \tau_{0.05})$ and $\tau_{0.5}$, and (e) transformation rate $\left(\frac{dV_c}{d\tau}\right)$ for $\tau_{0.5}$ of 0.2s with different Avrami index *n* values. The *X*-axis of panels (a) and (e) is in log scale to be consistent with the kinetics data.

at 20 °C higher temperatures in PA66. Given that mobility is equivalent, there must be other driving factors to control the thickening process.

The temperature-dependent numbers of nuclei for both polyamides were estimated using crystal size. The crystal size measured at T_c for several samples is estimated, as illustrated in Figures SI 5 and 6. It should be noted that the area estimation of low-temperature crystals may underestimate the overall size because no clear crystal center can be identified, and one fractional crystal may be miscounted as a whole crystal. Assuming all measured crystals have a sphere geometry (this may be incorrect since the Avrami index *n* is 2 at high T_cs), the measured area allows the estimation of equivalent spherical diameter (ESD) with the formula of $d = \sqrt{\frac{4A}{\pi}}$. The number of nucleation within a given volume is then calculated using the estimated ESD with an equation of $N = \frac{6}{\pi d^3}$. The size measurements support the previous discussion of transparent polarized micrographs at low T_cs that the average crystal size is smaller than the light wavelength (550 nm) when the temperature is below 125 °C for PA66 and 105 °C for PA6. The estimated nuclei density for both polyamides is estimated, as displayed in Figure 7. Representative AFM micrographs of PA66 and PA6 with the Avrami index *n* of 3 and 2 are added for comparison.

An abrupt break of nucleation density is found near the kinetics break temperature in both polyamides. PA6 heterogeneous nucleation data from Yaghini and Peters is added for comparison.[50] A drastic change of nucleation density follows the explanation of polymorphism transition since different polymorphs can have different nucleation energy barriers, determined in some polymers.[24] In the temperature range between 110 and 165 °C, the nucleation density of PA6 measured in this study is approximately 1 order of magnitude higher than the literature value. The discrepancy may be due to the assumption of continuity in the temperature coefficient of nucleation in the reference data extrapolation at such high undercooling or that this study underestimates the crystal area. A clear deviation between the literature and measured data occurs at 105 °C, suggesting that the traditional trend of nucleation density fails to represent the nucleation density below the kinetic transition temperature.

Effect of Avrami Index *n* on t_{peak} Value, Peak Height, and Peak Width. The Avrami analysis performed here has confirmed that the Avrami equation gives a good description of the primary crystallization kinetics with only *k*, *n*, and t_0 values. To simplify the discussion below, time since the crystallization onset defined as $\tau = t - t_0$ is used. Assuming that experimental data of primary crystallization always follows the Avrami equation, the normalized heat flow can be described by the first derivative of Avrami eq (2), given as

$$\frac{dV_c}{d\tau} = kn\tau^{n-1}e^{-k\tau^n} \tag{5}$$

The second derivative of Avrami eq (2) is

$$\frac{d^2V_c}{d\tau^2} = kn(n-1)\tau^{n-2}e^{-k\tau^n} - k^2n^2\tau^{2n-2}e^{-k\tau^n} \tag{6}$$

https://doi.org/10.1021/acs.macromol.2c01059
Macromolecules 2022, 55, 9220−9231

Then, the crystallization peak time τ_{peak} ($\equiv t_{peak} - t_0$) and peak height $\frac{dV_c(\tau=\tau_{peak})}{d\tau}$ are calculated using eqs (5 and 6), given as

$$\tau_{peak} = \left(\frac{n-1}{nk}\right)^{\frac{1}{n}} \tag{7}$$

$$\frac{dV_c(\tau=\tau_{peak})}{d\tau} = kn\left(\frac{n-1}{nk}\right)^{\frac{n-1}{n}} \exp\left(-\frac{n-1}{n}\right) \tag{8}$$

Since k is a function of $\tau_{0.5}$ ($\equiv t_{0.5} - t_0$) and n with the formula below

$$k = -\frac{\ln(0.5)}{\tau_{0.5}^{\,n}} \tag{9}$$

The formula for the first derivative of the Avrami equation, τ_{peak}, and peak height then becomes a function of $\tau_{0.5}$, as described as

$$\frac{dV_c}{d\tau} = -\frac{\ln(0.5)}{\tau_{0.5}^{\,n}} n\tau^{n-1} e^{\frac{\ln(0.5)}{\tau_{0.5}^{\,n}}\tau^n} \tag{10}$$

$$\tau_{peak} = \left(-\frac{n-1}{n}\frac{1}{\ln 0.5}\right)^{\frac{1}{n}} \tau_{0.5} \tag{11}$$

$$\frac{dV_c(\tau=\tau_{peak})}{d\tau} = -\frac{\ln 0.5}{\tau 0.5^n} n\left[-\frac{n-1}{n}\frac{\tau_{0.5}^{\,n}}{\ln 0.5}\right]^{\frac{n-1}{n}} \exp\left(-\frac{n-1}{n}\right) \tag{12}$$

Assuming the peak width equals to time between 95% transformation time and 5% transformation time, then the $\tau_{0.05}$, $\tau_{0.95}$, and $\tau_{width}/\tau_{0.5}$ values are equal to

$$\tau_{0.05} = \left(\frac{\ln 0.95}{\ln 0.5}\right)^{\frac{1}{n}} \tau_{0.5} \tag{13}$$

$$\tau_{0.95} = \left(\frac{\ln 0.05}{\ln 0.5}\right)^{\frac{1}{n}} \tau_{0.5} \tag{14}$$

$$\tau_{width} = \left[\left(\frac{\ln 0.95}{\ln 0.5}\right)^{\frac{1}{n}} - \left(\frac{\ln 0.05}{\ln 0.5}\right)^{\frac{1}{n}}\right] \tau_{0.5} \tag{15}$$

In Figure 8a, the parameters of τ_{peak}, $\tau_{0.5}$, peak height $\left(\frac{dV_c(t=\tau_{peak})}{d\tau}\right)$, $\tau_{0.05}$, $\tau_{0.95}$, and τ_{width} discussed above are illustrated.

Using the formulae above, if the primary crystallization of the polymer follows the Avrami equation, one can draw many interesting conclusions. It is often assumed that the peak time equals the half-transformation time. However, the discrepancy is sometimes observed between the measured t_{peak} values and $t_{0.5}$ values, even if both values have the same induction time. For example, in a previous study of PA6, the measured t_{peak} value and $t_{0.5}$ values show slight differences.[8] Using eq (11), the ratio of τ_{peak} and $\tau_{0.5}$ is only a function of n. Their relationship is plotted in Figure 8b; τ_{peak} equals $\tau_{0.5}$ only when n is 3.26. If the n value is 3 or above, the difference between τ_{peak} and $\tau_{0.5}$ is always less than 5%, suggesting that the former assumption is mostly accurate. A large discrepancy between τ_{peak} and $\tau_{0.5}$ is expected to occur when n is smaller, such as higher T_cs. Using eq (12), for a given $\tau_{0.5}$ and n, the peak height $\left(\frac{dVc(\tau=\tau_{peak})}{d\tau}\right)$ is calculated and plotted in Figure 8c, which leads to the conclusion that faster crystallization (smaller $\tau_{0.5}$) and higher n value give a sharper peak. This agrees with our observations from the waterfall plots for PA66 and PA6: within the same crystalline phase region, faster crystallization has a sharper peak; after a step change from n = 3 to 2, the peak becomes significantly lower. Using eq (15), a universal conclusion of peak width can be drawn, as illustrated in Figure 8d. That is, the peak width is always narrower at higher n.

To better visualize the effect of n on the crystallization conversion rate $\frac{dVc}{dt}$, peaks with $\tau_{0.5}$ of 0.2 s and different n values are reconstructed, as illustrated in Figure 8e. The dashed line of 0.2 s is added as a reference to compare with the peak time. The discrepancy between τ^{peak} and $\tau_{0.5}$ is apparent when n is below 2.5. The broadening of the peak is pronounced when n is lower even though they all have the same $\tau_{0.5}$.

From the Avrami analyses and morphological characterizations in this work, a clear sudden change of n associated with polymorphism transition is obtained. The mathematical discussion above can well explain observations from two polyamides. Since many thermoplastics undergo a mesophase-thermodynamical stable phase transition at the kinetics break, it is believed that a similar sudden change in n will occur, as found in iPP by De Santis et al.[12] Hence, the sudden broadening should be universal for all thermoplastics that exhibit a bimodal change of crystallization kinetics.

CONCLUSIONS

This work studies and reconsiders the descriptors inherent in the Avrami analysis as well as the overall isothermal crystallization peak shape to capture a more complete understanding of crystallization kinetics and morphology of PA66 and PA6 at high undercooling conditions. This objective was achieved using a novel FSC chip, allowing nondestructive AFM morphology characterization. From isothermal crystallization kinetics analysis, PA66 crystallizes much faster than PA6 in the entire temperature range regardless of morphology or polymorphs, supported by the temperature-dependent Avrami kinetics coefficients k. In both samples, bimodal crystallization kinetics were observed. The data show a break of kinetics at the local crystallization rate minimum at 130 °C for PA66 and at 105 °C for PA6. A sudden broadening of the exothermic crystallization peak occurs near the kinetics break temperature coinciding with the change in microstructure. Near the kinetics break, the Avrami indices n undergo a step change from 3 to 2 with increasing temperature, and the Avrami kinetics coefficient k for both polyamides shows two distinct temperature-dependent trends. The k value of PA66 is always at least 1 order of magnitude larger than PA6 and 2−3 orders over most of the temperature range for crystal formation, indicating far-faster crystallization.

The polarized micrographs of both polyamides show a transition from totally dark to having some visible crystals as T_c increases. The transition takes place near the kinetics break temperature. The change in transparency is associated with increasing crystal size and a more considerable refractive index difference between the crystal and amorphous domains.

https://doi.org/10.1021/acs.macromol.2c01059
Macromolecules 2022, 55, 9220−9231

AFM data indicate that both polyamides go through multistage morphological changes from amorphous-like morphology, cauliflower-like crystals, crystal aggregates, and lamellar structure after T_c changes from near T_g to above the kinetics break temperature. Morphological transitions in PA66 always occur roughly 20 °C higher than in PA6. The 20 °C difference in transition temperatures is caused by the difference in their nucleation driving forces rather than different mobilities. AFM has also confirmed that the crystal size and nucleation density change significantly near the transition temperature. The kinetics and morphological observations demonstrate that bimodal kinetics are caused by polymorphism transition.

Finally, the Avrami analysis has indicated that the Avrami index n also describes the ratio of τ_{peak} and $\tau_{0.5}$, peak height, as well as peak width. The sudden broadening of the exothermic peak is related to a step decrease of the Avrami index n. The crystallization exotherm peak broadening observed for many thermoplastics may be explained by the Avrami analysis similar to that performed here for PA66 and PA6.

■ ASSOCIATED CONTENT

Supporting Information

The Supporting Information is available free of charge at https://pubs.acs.org/doi/10.1021/acs.macromol.2c01059.

> Exothermic heat flow with baseline during isothermal crystallization of PA66 and PA6 at indicated temperatures; Avrami plot of PA66 experimental data obtained from isothermal crystallization between 140 and 180 °C; kinetic parameters for PA66 and PA6; melting curves of PA66 and PA6 after crystallization at 85 °C for 120 s; and PA66 and PA6 crystal size estimation using AFM micrographs and ImageJ (PDF)

■ AUTHOR INFORMATION

Corresponding Author

Alicyn Rhoades − *School of Engineering, Penn State Behrend, Erie, Pennsylvania 16563, United States;* orcid.org/0000-0003-4678-419X; Email: amh234@psu.edu

Authors

Xiaoshi Zhang − *School of Engineering, Penn State Behrend, Erie, Pennsylvania 16563, United States;* orcid.org/0000-0002-5281-6285

John Buzinkai − *INVISTA, Wichita, Kansas 67220, United States*

Evan Quinn − *School of Engineering, Penn State Behrend, Erie, Pennsylvania 16563, United States*

Complete contact information is available at: https://pubs.acs.org/10.1021/acs.macromol.2c01059

Notes

The authors declare no competing financial interest.

■ ACKNOWLEDGMENTS

This research was funded by INVISTA and the National Science Foundation (Grant #1653629). The discussion with Anne Gohn was gratefully acknowledged.

■ REFERENCES

(1) Murthy, N. S. Hydrogen Bonding, Mobility, and Structural Transitions in Aliphatic Polyamides. *J. Polym. Sci., Part B: Polym. Phys.* **2006**, *44*, 1763−1782.

(2) Krause, B.; Kroschwald, L.; Pötschke, P. The Influence of the Blend Ratio in PA6/PA66/MWCNT Blend Composites on the Electrical and Thermal Properties. *Polymers* **2019**, *11*, 122.

(3) Palmer, R. J.; by Staff, U.. Polyamides, Plastics. In *Kirk-Othmer Encyclopedia of Chemical Technology*; American Cancer Society, 2005 DOI: 10.1002/0471238961.1612011916011213.a01.pub2.

(4) Matsuda, T.; Shimomura, T.; Hirami, M. Crystallization and Melting of Binary Mixtures of Nylon 6 and Nylon 66. A Study by DSC. *Polymer Journal* **1999**, *31*, 795−800.

(5) ISO 1874-2:2012. *Plastics — Polyamide (PA) Moulding and Extrusion Materials — Part 2: Preparation of Test Specimens and Determination of Properties*.

(6) Rhoades, A. M.; Williams, J. L.; Androsch, R. Crystallization Kinetics of Polyamide 66 at Processing-Relevant Cooling Conditions and High Supercooling. *Thermochim. Acta* **2015**, *603*, 103−109.

(7) Gohn, A. M.; Rhoades, A. M.; Wonderling, N.; Tighe, T.; Androsch, R. The Effect of Supercooling of the Melt on the Semicrystalline Morphology of PA 66. *Thermochim. Acta* **2017**, *655*, 313−318.

(8) Zhang, X.; Gohn, A.; Mendis, G.; Buzinkai, J. F.; Weigand, S. J.; Rhoades, A. M. Probing Three Distinct Crystal Polymorphs of Melt-Crystallized Polyamide 6 by an Integrated Fast Scanning Calorimetry Chip System. *Macromolecules* **2021**, *54*, 7512−7528.

(9) Mileva, D.; Kolesov, I.; Androsch, R. Morphology of Cold-Crystallized Polyamide 6. *Colloid Polym. Sci.* **2012**, *290*, 971−978.

(10) Jiang, Q.; Zhao, Y.; Zhang, C.; Yang, J.; Xu, Y.; Wang, D. In-Situ Investigation on the Structural Evolution of Mesomorphic Isotactic Polypropylene in a Continuous Heating Process. *Polymer* **2016**, *105*, 133−143.

(11) Toda, A.; Androsch, R.; Schick, C. Insights into Polymer Crystallization and Melting from Fast Scanning Chip Calorimetry. *Polymer* **2016**, *91*, 239−263.

(12) de Santis, F.; Adamovsky, S.; Titomanlio, G.; Schick, C. Isothermal Nanocalorimetry of Isotactic Polypropylene. *Macromolecules* **2007**, *40*, 9026−9031.

(13) Rhoades, A. M.; Wonderling, N.; Schick, C.; Androsch, R. Supercooling-Controlled Heterogeneous and Homogenous Crystal Nucleation of Polyamide 11 and Its Effect onto the Crystal/Mesophase Polymorphism. *Polymer* **2016**, *106*, 29−34.

(14) Androsch, R.; Rhoades, A. M.; Stolte, I.; Schick, C. Density of Heterogeneous and Homogeneous Crystal Nuclei in Poly (Butylene Terephthalate). *Eur. Polym. J.* **2015**, *66*, 180−189.

(15) Seo, J.; Gohn, A. M.; Dubin, O.; Takahashi, H.; Hasegawa, H.; Sato, R.; Rhoades, A. M.; Schaake, R. P.; Colby, R. H. Isothermal Crystallization of Poly(Ether Ether Ketone) with Different Molecular Weights over a Wide Temperature Range. *Polym. Cryst.* **2019**, *2*, No. e10055.

(16) Rhoades, A. M.; Gohn, A. M.; Seo, J.; Androsch, R.; Colby, R. H. Sensitivity of Polymer Crystallization to Shear at Low and High Supercooling of the Melt. *Macromolecules* **2018**, *51*, 2785−2795.

(17) Kolesov, I.; Mileva, D.; Androsch, R.; Schick, C. Structure Formation of Polyamide 6 from the Glassy State by Fast Scanning Chip Calorimetry. *Polymer* **2011**, *52*, 5156−5165.

(18) Cavallo, D.; Gardella, L.; Alfonso, G. C.; Portale, G.; Balzano, L.; Androsch, R. Effect of Cooling Rate on the Crystal/Mesophase Polymorphism of Polyamide 6. *Colloid Polym. Sci.* **2011**, *289*, 1073−1079.

(19) Mollova, A.; Androsch, R.; Mileva, D.; Schick, C.; Benhamida, A. Effect of Supercooling on Crystallization of Polyamide 11. *Macromolecules* **2013**, *46*, 828−835.

(20) Schick, C.; Androsch, R.; Schmelzer, J. W. P. Homogeneous Crystal Nucleation in Polymers. *J. Phys.: Condens. Matter* **2017**, *29*, No. 453002.

(21) Massa, M. V.; Dalnoki-Veress, K. Homogeneous Crystallization of Poly(Ethylene Oxide) Confined to Droplets: The Dependence of

the Crystal Nucleation Rate on Length Scale and Temperature. *Phys. Rev. Lett.* **2004**, *92*, No. 255509.
(22) Michell, R. M.; Müller, A. J. Confined Crystallization of Polymeric Materials. *Prog. Polym. Sci.* **2016**, *54*−*55*, 183−213.
(23) Carvalho, J. L.; Dalnoki-Veress, K. Homogeneous Bulk, Surface, and Edge Nucleation in Crystalline Nanodroplets. *Phys. Rev. Lett.* **2010**, *105*, No. 237801.
(24) Zhang, X.; Marxsen, S. F.; Ortmann, P.; Mecking, S.; Alamo, R. G. Crystallization of Long-Spaced Precision Polyacetals II: Effect of Polymorphism on Isothermal Crystallization Kinetics. *Macromolecules* **2020**, *53*, 7899−7913.
(25) Marxsen, S. F.; Häußler, M.; Mecking, S.; Alamo, R. G. Crystallization of Long-Spaced Precision Polyacetals III: Polymorphism and Crystallization Kinetics of Even Polyacetals Spaced by 6 to 26 Methylenes. *Polymers* **2021**, *13*, No. 1560.
(26) Mileva, D.; Androsch, R.; Zhuravlev, E.; Schick, C. Morphology of Mesophase and Crystals of Polyamide 6 Prepared in a Fast Scanning Chip Calorimeter. *Polymer* **2012**, *53*, 3994−4001.
(27) Oshinski, A. J.; Keskkula, H.; Paul, D. R. The Role of Matrix Molecular Weight in Rubber Toughened Nylon 6 Blends: 1. Morphology. *Polymer* **1996**, *37*, 4891−4907.
(28) Illers, V. K.-H.; Haberkorn, H. Schmelzverhalten, Struktur Und Kristallinität von 6-Polyamid. *Makromol. Chem.* **1971**, *142*, 31−67.
(29) Seo, J.; Takahashi, H.; Nazari, B.; Rhoades, A. M.; Schaake, R. P.; Colby, R. H. Isothermal Flow-Induced Crystallization of Polyamide 66 Melts. *Macromolecules* **2018**, *51*, 4269−4279.
(30) Krause, B.; Kroschwald, L.; Pötschke, P. The Influence of the Blend Ratio in PA6/PA66/MWCNT Blend Composites on the Electrical and Thermal Properties. *Polymers* **2019**, *11*, No. 122.
(31) van Drongelen, M.; Meijer-Vissers, T.; Cavallo, D.; Portale, G.; Poel, G. vanden.; Androsch, R. Microfocus Wide-Angle X-Ray Scattering of Polymers Crystallized in a Fast Scanning Chip Calorimeter. *Thermochim. Acta* **2013**, *563*, 33−37.
(32) Turnbull, D.; Fisher, J. C. Rate of Nucleation in Condensed Systems. *J. Chem. Phys.* **1949**, *17*, 71−73.
(33) Avrami, M. Kinetics of Phase Change. I: General Theory. *J. Chem. Phys.* **1939**, *7*, 1103−1112.
(34) Avrami, M. Kinetics of Phase Change. II Transformation-Time Relations for Random Distribution of Nuclei. *J. Chem. Phys.* **1940**, *8*, 212−224.
(35) Suzuki, A.; Murata, H.; Kunugi, T. Application of a High-Tension Annealing Method to Nylon 66 Fibres. *Polymer* **1998**, *39*, 1351−1355.
(36) Inoue, K.; Hoshino, S. Effect of Molecular Orientation on the Swelling of Nylon 6. *J. Polym. Sci., Polym. Phys. Ed.* **1977**, *15*, 1363−1378.
(37) Lorenzo, A. T.; Arnal, M. L.; Albuerne, J.; Müller, A. J. DSC Isothermal Polymer Crystallization Kinetics Measurements and the Use of the Avrami Equation to Fit the Data: Guidelines to Avoid Common Problems. *Polym. Test.* **2007**, *26*, 222−231.
(38) Turska, E.; Gogolewski, S. Study on Crystallization of Nylon-6 (Polycapramide): Part 2. Effect of Molecular Weight on Isothermal Crystallization Kinetics. *Polymer* **1971**, *12*, 629−641.
(39) Androsch, R.; di Lorenzo, M. L.; Schick, C.; Wunderlich, B. Mesophases in Polyethylene, Polypropylene, and Poly(1-Butene). *Polymer* **2010**, *51*, 4639−4662.
(40) Patel, R. M.; Spruiell, J. E. Crystallization Kinetics during Polymer Processing—Analysis of Available Approaches for Process Modeling. *Polymer Eng. Sci.* **1991**, *31*, 730−738.
(41) Rwei, S. P.; Tseng, Y. C.; Chiu, K. C.; Chang, S. M.; Chen, Y. M. The Crystallization Kinetics of Nylon 6/6T and Nylon 66/6T Copolymers. *Thermochim. Acta* **2013**, *555*, 37−45.
(42) Albano, C.; Sciamanna, R.; Gónzalez, R.; Papa, J.; Navarro, O. Analysis of Nylon 66 Solidification Process. *Eur. Polym. J.* **2001**, *37*, 851−860.
(43) Mandelkern, L.*Crystallization of Polymers: Volume 2, Kinetics and Mechanisms*; Cambridge University Press: Cambridge, U.K.; 2004.
(44) Piorkowska, E.; Galeski, A.; Haudin, J.-M. Critical Assessment of Overall Crystallization Kinetics Theories and Predictions. *Prog. Polym. Sci.* **2006**, *31*, 549−575.
(45) Lin, Y.; Bilotti, E.; Bastiaansen, C. W. M.; Peijs, T. Transparent Semi-Crystalline Polymeric Materials and Their Nanocomposites: A Review. *Polym. Eng. Sci.* **2020**, *60*, 2351−2376.
(46) Fouda, I. M.; El-Tonsy, M. M.; Hosny, H. M.; Metawe, F. M.; Easawi, K. H. Optothermal Properties of Fibers. X. Temperature Dependence of the Skin—Core Structure of Nylon-6 Fibers. *J. Appl. Polym. Sci.* **1997**, *66*, 695−709.
(47) Founda, I. M.; El-Nicklawy, M. M.; Nasr, E. M.; El-Agamy, R. M. Optothermal Properties of Fibers. III. Optical Anisotropy in Nylon 66 Fibers as a Function of Annealing Process. *J. Appl. Polym. Sci.* **1996**, *60*, 1247−1267.
(48) Groh, W.; Zimmermann, A. What Is the Lowest Refractive Index of an Organic Polymer? *Macromolecules* **1991**, *24*, 6660−6663.
(49) Strobl, G. From the Melt via Mesomorphic and Granular Crystalline Layers to Lamellar Crystallites: A Major Route Followed in Polymer Crystallization? *Eur. Phys. J. E* **2000**, *3*, 165−183.
(50) Yaghini, N.; Peters, G. W. M. Modeling Crystallization Kinetics and Resulting Properties of Polyamide 6. *Macromolecules* **2021**, *54*, 1894−1904.

https://doi.org/10.1021/acs.macromol.2c01059
Macromolecules 2022, 55, 9220−9231